LIMNOLOGY
and
OCEANOGRAPHY

ASLO

Limnol. Oceanogr. 67, 2022, 527–539

doi: 10.1002/lno.12009

Net ecosystem dissolution and respiration dominate metabolic rates at two western Atlantic reef sites

Melissa Meléndez,[1*] **Joseph Salisbury**,[2] **Dwight Gledhill**,[3] **Chris Langdon**,[4] **Julio M. Morell**,[5,6] **Derek Manzello**,[7] **Adrienne Sutton**[8]

[1]Department of Oceanography, University of Hawai'i at Mānoa, Honolulu, Hawai'i
[2]Ocean Processes Analysis Laboratory, Department of Earth Sciences, University of New Hampshire, Durham, New Hampshire
[3]Ocean Acidification Program, NOAA, Silver Spring, Maryland
[4]Rosenstiel School of Marine and Atmospheric Science, University of Miami, Miami, Florida
[5]Department of Marine Sciences, University of Puerto Rico, Mayagüez, Puerto Rico
[6]Caribbean Coastal Ocean Observing System, Magueyes Island, Lajas, Puerto Rico
[7]Satellite Oceanography and Climate Division, Center for Satellite Applications and Research, NOAA, College Park, Maryland
[8]Pacific Marine Environmental Laboratory, NOAA, Seattle, Washington

Abstract

Ocean acidification is changing surface water chemistry, but natural variability due to nearshore processes can mask its effects on ecosystem responses. We present an approach of quantitatively resolving net ecosystem metabolism from an array of long-term time series stations, offering perhaps the longest record of such processes over a reef to date. We used 8 and 6 yr of in situ, high-quality frequency observations to characterize the changes in dissolved inorganic carbon and oxygen in La Parguera, Puerto Rico and Cheeca Rocks, Florida, respectively. Net respiration and net dissolution are the dominant metabolic processes at both systems, with a narrow window of ~ 4 months under net calcification. The annual mean net ecosystem calcification (NEC) rates for La Parguera (-0.68 ± 0.91 kg $CaCO_3$ m^{-2} yr^{-1}) and Cheeca Rocks (-0.48 ± 0.89 kg $CaCO_3$ m^{-2} yr^{-1}) were on the lower end of typical NEC ranges determined for other reef areas using chemistry- and census-based approaches. At Cheeca Rocks, 53% of the variance in NEC can be explained by net ecosystem production (NEP) and 30% by aragonite saturation state (Ω_{arag}). At La Parguera, NEC is primarily driven by changes in NEP. The linear relationship between NEC and NEP showed a significant slope (± standard error) of 1.00 ± 0.005 and 0.88 ± 0.04 for La Parguera and Cheeca Rocks, respectively. These results suggest that NEP appears to play a prominent role on NEC, and Ω_{arag} probably is not the most informative measure to monitor when attempting to resolve the long-term impacts of ocean acidification.

Surface ocean carbon chemistry is currently changing owing to the burning of fossil fuels (Friedlingstein et al. 2019). The increase in atmospheric carbon dioxide (CO_{2atm}) from anthropogenic activities has resulted in an increase in CO_2 in surface seawater (CO_{2sw}) and ocean acidification (Bates et al. 2012). Physical, chemical, and biological processes that influence the surface ocean concentration of CO_2 in nearshore areas complicate our understanding of the carbonate system (Duarte et al. 2013). Models for open-ocean waters in tropical systems (Gledhill et al. 2008) have helped characterize ocean acidification trends in open-ocean waters and have informed the debate about future ocean acidification conditions in coral reef areas (Cyronak et al. 2014). Nevertheless, current and future trends in ocean acidification are still unknown because of the difficulty associated with separating nearshore biogeochemical processes from total ocean changes in surface pH.

Direct observations at coral reef sites in the western Atlantic show significant changes in the coastal surface seawater carbonate chemistry relative to the global open ocean because of enhanced biological and temperature dynamics near the coast (Bates et al. 2012). It is critical to examine areas where substantial changes in carbonate chemistry are expected to occur (Andersson et al. 2019), especially those that are readily accessible or have ongoing related monitoring programs (Sutton et al. 2014, 2019). Coral reef areas in the western Atlantic, where surface waters are likely to be affected by ocean acidification and to warm sooner and more intensely than other reef

*Correspondence: mmelen@hawaii.edu

Additional Supporting Information may be found in the online version of this article.

regions, have experienced significant reductions in live coral cover, causing a shift from reefs dominated by scleractinian corals to algae-dominated reefs (Gardner et al. 2003). Characterization of the ecosystem metabolic response is essential if we are to understand the sensitivity of nearshore coral reefs to ocean acidification.

Biological processes driving CO_2 changes on diurnal and seasonal timescales include net ecosystem production (NEP) and net ecosystem calcification (NEC) from all autotrophic, heterotrophic, biotic, and abiotic components of the system. NEP is the difference between gross primary production and ecosystem respiration, and NEC is the difference between calcification and dissolution, as described in the following simplified equations (Gattuso et al. 1998):

$$CO_2 + H_2O \underset{\text{respiration}}{\overset{\text{photosynthesis}}{\rightleftharpoons}} CH_2O + O_2,$$

$$Ca^{2+} + CO_3^{2-} \underset{\text{dissolution}}{\overset{\text{calcification}}{\rightleftharpoons}} CaCO_3.$$

Calcification and organic respiration lead to increases in seawater partial pressure of CO_2 (pCO_{2sw}) and dissolved inorganic carbon (DIC) that can potentially reduce both the ocean pH and the ocean's ability to remove CO_2 from the atmosphere. The uptake of DIC via photosynthesis and the increase in total alkalinity (TA) via calcium carbonate ($CaCO_3$) dissolution both lower the surface pCO_{2sw} concentration and increase the buffering capacity of seawater.

Several methods are commonly used to measure NEP and NEC processes in nearshore surface waters. For example, net calcification and production measurements typically adopt various Lagrangian or Eulerian techniques requiring high-temporal resolution of discrete TA and DIC measurements in seawater (Albright et al. 2015). Recently, in situ autonomous methods have been proposed that offer great promise but currently remain cost-prohibitive and have a limited operating duration of a few weeks, at most, due to biofouling and sensor drift (Yates and Halley, 2003; Takeshita et al. 2016). Modeling NEP and NEC processes using carbon balance approaches have proven successful in surface open-ocean settings (Gruber et al. 1998; Shadwick et al. 2011). The adoption of this technique has been limited in coastal zones partially because of the limited number of direct high-frequency observations available to quantitatively separate processes affecting CO_2 and capture the fast timescales of coastal processes. We identified only two coral reef time series in the western Atlantic (Sutton et al. 2019) with temporal spans that were adequate for detecting seasonal trends and were accompanied by auxiliary data to quantitatively estimate the magnitude of NEP and NEC based on the temporal evolution of oxygen (O_2) and DIC.

In this study, an existing mass balance approach for CO_2 (Gruber et al. 1998) is implemented, refined, and expanded to decouple organic and inorganic metabolism (NEP and NEC) using pCO_2, DIC, and O_2 as proxies. We apply this diagnostic technique to a one-dimensional (1D) mass balance model using CO_2 climate quality (Newton et al. 2015) and high-frequency (3-h) carbonate observations spanning 6–8 yr from two shallow nearshore reef areas in Florida and Puerto Rico. The model assumes an open system and well-mixed water column to provide an integrated assessment of biogeochemical variability over time within a water parcel close to the buoy (< 5 km). Our ecosystem metabolic rates integrate over extended periods (months to years) and are representative of multiple habitats. We compare and contrast our results with previous studies in Florida and Puerto Rico using chemistry- and census-based approaches. We also evaluated the correlation between NEC and NEP to provide information about the role of organic metabolism in NEC and our ability to define geochemical thresholds at which dissolution exceeds calcification (Andersson and Gledhill 2013). Given the decline in carbonate production reported for the Caribbean reefs (Perry et al. 2013), we expect that both locations exhibit low NEC that is closely linked to low coral cover, sediment dissolution, high temperatures and organic carbon inputs.

Methods

Study sites

The buoy in Puerto Rico is located in La Parguera Natural Marine Reserve at the southwest end of the Enrique mid-shelf reef. The buoy in Florida is in the upper Florida Keys National Marine Sanctuary over Cheeca Rocks, an isolated nearshore patch reef. Both buoys are in shallow areas (3 m depth) approximately 2 km off the coast (Fig. 1).

The spatiotemporal scales of the La Parguera buoy cover approximately 0.5 km of the Enrique forereef over a semidiurnal cycle (12 h) due to the low current speed observed in the area (0.05 km h^{-1}) and the predominant southwest direction (Fig. 1). Forereef benthic calcifiers (Supporting Information Table S1) include octocorals (26%), hard corals (10–11%), and crustose coralline algae (1%). No secondary (calcareous encrusters) or sediment (calcareous algae such as *Halimeda* or benthic foraminifera) producers were found during multiple visual surveys (Moyer et al. 2012). The percentage of the total forereef area covered by benthic primary producers (e.g., cyanobacteria, macroalgae, and turf algae) is 17%. Carbonate sand, rubble, and rock (35%) are the dominant abiotic components in this area. *Rhizophora mangle* and *Laguncularia racemosa* mangroves have colonized the Enrique reef crest. The inorganic nutrient concentrations across the Caribbean and La Parguera coral reefs are low (Meléndez et al. 2020). Riverine influence is at its minimum during the winter and spring, while the Amazon and Orinoco plumes dominate the southeastern Caribbean during the summer and fall (Corredor and

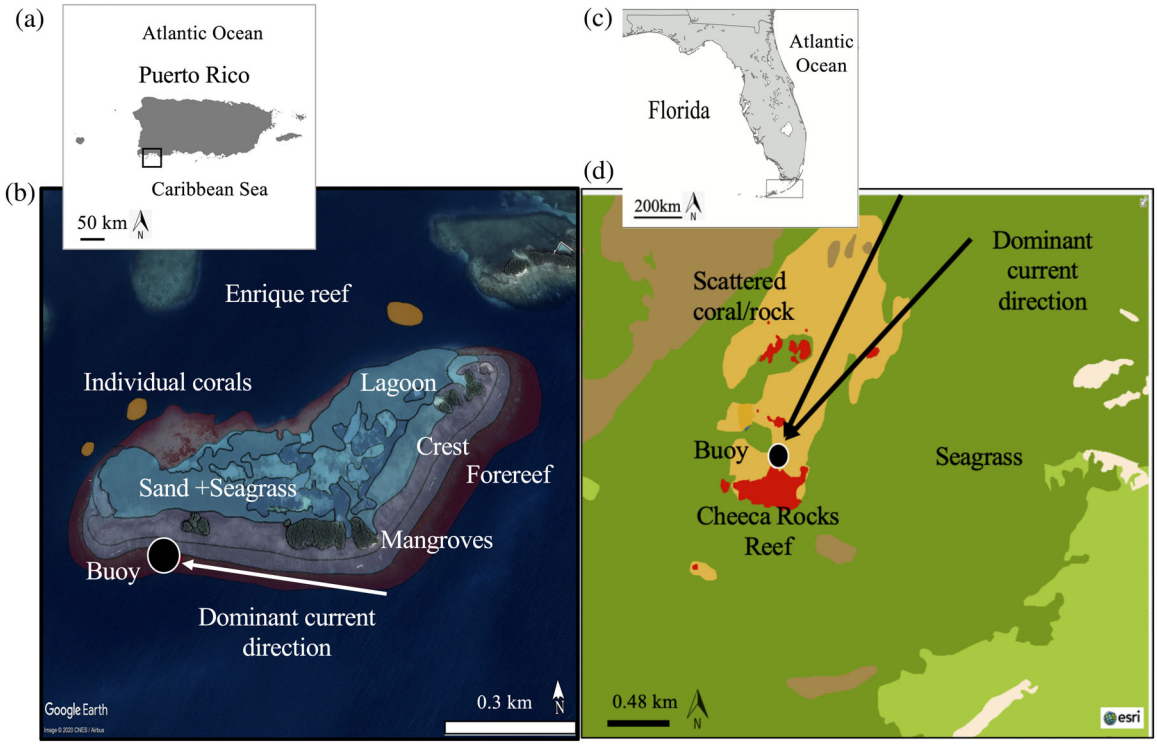

Fig. 1. (**a**) Map showing the island of Puerto Rico and the marine protected area of La Parguera (box). (**b**) Over the forereef (red path) at the west end of the Enrique reef (17.95°N, 67.05°W) is the La Parguera MapCO_2 buoy (black circle). The white arrow direction and length (~ 0.5 km) indicate the dominant current direction and speed (0.04 km h^{-1}), respectively. The Enrique forereef extends 1.32 km along a northeast-southeast axis. Individual corals (orange path), sand, and seagrass beds (light blue path) are present in the lagoon area. Red mangroves have colonized the reef crest (pink path), composed mostly of coral rubble. (**c**) Map of the Upper Florida Reef Tract (box). (**d**) North of the Cheeca Rocks patch reef is the MapCO_2 buoy (24.90°N, 80.62°W). The black arrow directions and lengths (~ 2 km) indicate the dominant current direction and speed (0.3 km h^{-1}), respectively. The red path indicates individual corals or aggregated patch reefs, and the green and brown paths represent seagrass and pavement, respectively. We use the ArcGIS Online Map Viewer to describe the benthic habitats for the Florida Keys National Marine Sanctuary (Taylor et al. 2018) and Puerto Rico (Kendall et al. 2001).

Morell, 2001). The average seawater temperature at La Parguera ranged from 27.1 ± 0.2°C in winter to 29.7 ± 0.3°C in summer.

The predominant current direction at the Cheeca Rocks buoy is southward (Meléndez et al. 2020), with a maximum current speed of 0.3 km h^{-1} (Fig. 1). The spatiotemporal coverage over a semidiurnal cycle is approximately 3 km. The benthic communities located north of the buoy include hard bottom areas with fine-grained $CaCO_3$ sediments, some isolated hard and soft corals, and seagrass. Surveys at the Cheeca Rocks buoy site show that macroalgae (46.6%) and hard coral (25.5–33%) dominate the benthic composition, followed by 6.5% sand, 6.1% secondary carbonate producers, and 1–3% soft corals (Supporting Information Table S1). The tidal exchanges can also send pulses of Florida Bay water into inner reef areas through different tidal channels, particularly during the winter (Smith and Lee, 2003). The bay consists primarily of shallow (< 8 m) seagrass and sand environments, with occasional, isolated patch reefs intermixed (Jones, 1977). The average seawater temperature at Cheeca Rocks ranged from 23.4 ± 0.9°C in winter to 30.6 ± 0.5°C in summer.

Autonomous observations

The Pacific Marine Environmental Laboratory (PMEL) time series includes a moored autonomous pCO_2 system (MapCO_2) that provides 3-h measurements of both pCO_{2air} and pCO_{2sw}, sea surface salinity (SSS) and sea surface temperature (SST), pH, and O_2. The buoys have a seawater–gas equilibrator, a reference gas standard, an infrared gas analyzer, a sea-bird conductivity and temperature recorder (SBE 16 SeaCAT), a SAMI-pH system, and an O_2 optode (Aanderaa 4775) at approximately 1 m depth. The overall uncertainty in autonomous pCO_{2sw} is <2 μatm (Sutton et al. 2014). We used autonomous measurements from January 2009 (La Parguera) and November 2011 (Cheeca Rocks) to September 2017.

An internal Maxtec™ oxygen sensor (MAX-250+) is inside the CO_2 electronics tube to measure the percentage of oxygen in the air (% O_2) and is used primarily for the MapCO_2 system diagnostic, but has also been applied to studying ocean biological variability (Massaro et al. 2012; Xue et al. 2016). In this study, the autonomous measurements made by the MAX-250+ oxygen were post-calibrated using the slope and offset of the

linear correlation with the higher-quality O_2 optode measurements (Meléndez et al. 2020) to derive daily NEP. We preferred this method over using the oxygen optode measurements to estimate seasonal NEP, as MAX-250+ does not present issues related to sensor drift and temporal coverage is higher than the optodes (Meléndez et al. 2020). The final uncertainties in the corrected MAX-250+ oxygen values were ±6 and ±7 μmol kg^{-1} for La Parguera and Cheeca Rocks, respectively.

Discrete observations

Monitoring at these stations includes laboratory-based, high-precision determinations of potentiometric TA, infrared DIC or spectrophotometric pH. High-quality direct measurements of TA (± 1–3 μmol kg^{-1}), DIC (± 2 μmol kg^{-1}), and pH (± 0.006) were available at each site to fully constrain the carbonate system, and for validation and quality assurance/control processes. Data were available for all seasons. For a complete description of the discrete surveys, the intervals of available data from autonomous and discrete observations refer to Meléndez et al. (2020).

Modeled carbonate parameters

Regional TA–salinity relationships (Lee et al. 2006) tend to break down for nearshore waters subject to freshwater inputs and biological activity; therefore, site-specific relationships must be determined (see Supporting Information Text S1 for further details). The resultant multivariate linear relationship for La Parguera (TA_{LP}) and Cheeca Rocks (TA_{CR}) are:

$$TA_{LP} = 43.2 \times SSS - 12.5 \times SST + 1118.1, \quad (1)$$

$$TA_{CR} = 2.2 \times SSS - 11.8 \times SST + 2612.7. \quad (2)$$

The modeled uncertainty in TA at La Parguera and Cheeca Rocks were 30 and 47 μmol kg^{-1}, respectively. We used pCO_{2sw} and TA to calculate the Ω_{arag}, which had a final uncertainty of 2% (La Parguera) and 4% (Cheeca Rocks), using the CO2SYS (van Heuven et al. 2011) modeling program of Orr et al. (2018). We applied the K_1 and K_2 dissociation constants of Lueker et al. (2000) and K_{HSO4-} from Dickson (1990). The solubility constant used to derive Ω_{arag} was from Mucci (1983). Even though the uncertainties in the modeled TA were high, due primarily to calcification and dissolution (Meléndez et al. 2020), the method used here to calculate Ω_{arag} yielded uncertainties that were within the "weather" goal targets (Newton et al. 2015).

Statistical analyses and seasonal changes

We removed high-frequency events, low-amplitude trends, and episodic events before calculating daily averages using a 33-h low-pass filter (Flagg et al. 1976). We define "high-frequency" as those events occurring at 24 h. We seek to decrease the bias that episodic events and random noise can produce, and eliminate signals affecting pCO_{2sw} occurring at sub-daily frequencies such as semidiurnal tides and diurnal heat flux. High-frequency variability affected the seasonal pCO_{2sw} amplitude by 4.5% at Cheeca Rocks, and 0.1% at La Parguera.

Average daily observations were used to construct the annual climatology of the measured and modeled parameters (see Supporting Information Table S2 for a list of the parameters used). The composite year was constructed by binning the data within the representative Julian day. The seasonal variability was computed using the peak-to-peak amplitude and compiled into four distinct seasons: winter (January–March), spring (April–June), summer (July–September), and fall (October–December). Parametric Student *t*-tests ($\alpha = 0.05$ significance level) were used to ascertain significance between seasons and differences observed between sites.

Numerical approach: Diagnostic single box mass balance model

To constrain the variability in air–sea exchange, mixing, and biological activity, we assumed an open system and calculated the daily changes in the initial observed values of in situ pCO_{2sw}. The carbonic acid system was derived and manipulated using the CO2SYS computer software program (van Heuven et al. 2011) using measured in situ pCO_{2sw} and modeled reef TA (Eqs. 1 and 2).

A 1D carbon mass balance model (Gruber et al. 1998; Shadwick et al. 2011; Fassbender et al. 2016) was used to calculate the net change in surface pCO_{2sw} (δpCO_{2OBS}) based on the daily partial changes (∂t) due to gas solubility as a function of temperature and salinity (SOL), air–sea exchange (AIR–SEA EX), mixing processes (HOR MIX), and biology (BIO). The biological term includes water column and benthic organic and inorganic fluxes. Figure 2 shows a schematic diagram of the open carbon box model and the processes assumed to affect NEP and NEC over time within a mixed water parcel close to the buoy. The following equation describes the mass balance of δpCO_{2OBS}:

$$\frac{\delta pCO_{2OBS}}{dt} = \frac{\partial pCO_{2\,SOL}}{\partial t} + \frac{\partial pCO_{2\,AIR-SEA\,EX}}{\partial t} + \frac{\partial pCO_{2\,HOR\,MIX}}{\partial t} + \frac{\partial pCO_{2BIO}}{\partial t}. \quad (3)$$

Thermodynamic variability

The CO2SYS program was used to calculate ∂pCO_{2SOL} using observed daily changes in temperature and salinity. We preferred this method over the temperature-only dependence coefficient (0.0423°C^{-1}) by Takahashi et al. (1993) because both temperature and salinity create thermodynamic variability in these regions, and the temperature distributions are very different from those in the North Atlantic waters on which this dependence was derived.

Physical transport

The variation attributable to horizontal transport via advection ($\partial pCO_{2HOR\ MIX}$) was characterized empirically using daily salinity changes with assumed conservative mixing of the TA

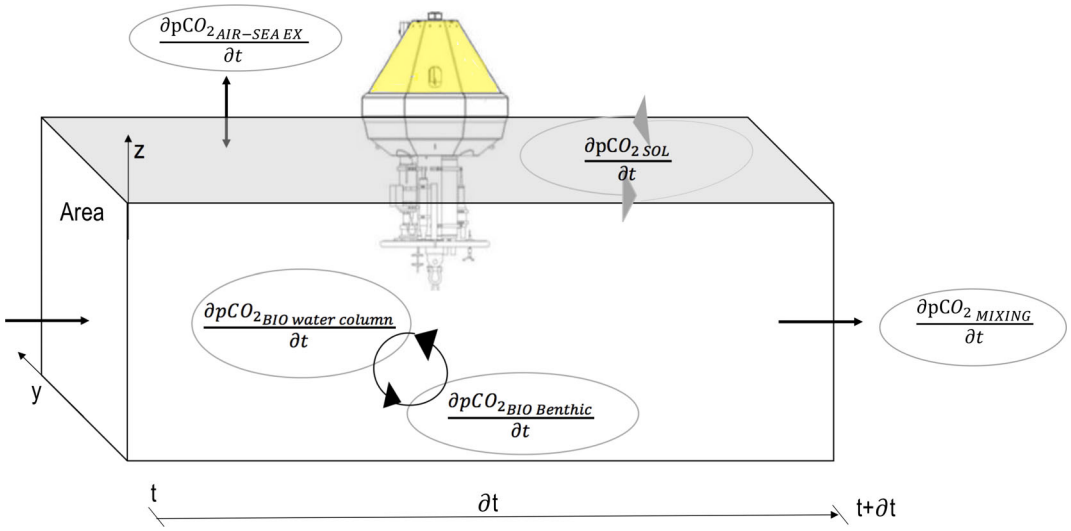

Fig. 2. Schematic diagram of the open CO_2 system box model. The net change in surface pCO_{2sw} is based on ∂pCO_2 due to gas solubility (SOL), air–sea exchange (AIR–SEA EX), mixing processes (HOR MIX), and biological activity (BIO) from organic and inorganic benthic and water column fluxes. ∂t is the change between t_1 and t_2. The fluxes are normalized to square meters of the seafloor and integrated through the mixed layer depth.

and DIC between the reef and open ocean (Xue et al. 2016). Note that the freshwater contributions from the Amazon River to both the North and South Atlantic oceans do not appear to be sufficient to alter the slope of the TA–salinity relationship (Cai et al. 2010). Therefore, we did not explicitly consider the slope–discharge relationships because according to the linear DIC–salinity and TA–salinity relationships at these sites, the ocean slopes are minimally affected by freshwater inputs and follow the end-member mixing line. The ocean end-member was determined from discrete TA and DIC samples obtained on seasonal cruises (Supporting Information Fig. S2) around the Caribbean and Atlantic regions as follows:

$$\mathrm{TA_{Caribbean}}(\pm 5) = 58.8 \times \mathrm{SSS} + 242, \quad (4)$$

$$\mathrm{DIC_{Caribbean}}(\pm 12) = 55.8 \times \mathrm{SSS} + 1.84, \quad (5)$$

$$\mathrm{TA_{Florida\ Straits}}(\pm 3) = 83.8 \times \mathrm{SSS} - 660, \quad (6)$$

$$\mathrm{DIC_{Florida\ Straits}}(\pm 6) = 77.1 \times \mathrm{SSS} - 771, \quad (7)$$

where ± 5, ± 12, ± 3, and ± 6 are the root mean square errors (RMSEs) of the derived quantity. The slopes of the TA–salinity relationship estimated here were similar to the results of Cai et al. (2010) for the Caribbean and Florida Straits (more details in Supporting Information Text S2). We used discrete TA and DIC measurements from the third Gulf of Mexico Ecosystems and Carbon Cycle cruise along the new 80.6°W transect between Cuba and Florida (Barbero et al. 2019), potentially capturing Gulf Stream water that flows northward before passing to the Cheeca Rocks buoy. Strong linear correlations between TA–salinity and DIC–salinity were observed ($r^2 > 0.95$), supporting the assumption of conservative mixing mechanisms between freshwater and seawater end-members in these regions (Supporting Information Fig. S2). Measurements were taken in August 2017, and those taken at <50 m depth were selected based on the buoyancy frequency (also known as Brunt–Väisälä frequency).

Changes due to vertical mixing were neglected, and the mixed layer (3 m) was assumed to extend to the bottom given the small variations in salinity and temperature observed from Conductivity, Temperature and Depth (CTD) casts performed during the discrete surveys, as well as the shallowness of the sites (Supporting Information Text S3). The seasonal change in salinity due to the mean potential evapotranspiration to precipitation rate was assumed to be small (< 0.1%) and hence neglected. The semidiurnal tides at La Parguera and Cheeca Rocks exhibited amplitudes of approximately 10–20 cm s^{-1} and oscillated about the mean tidal range (< 0.25 m) of the low-frequency spectrum. The contributions from short-term advection to salinity variability were assumed to be small at both sites.

Air–sea exchange

The air–sea CO_2 exchange ($\partial pCO_{2\mathrm{AIR-SEA\ EX}}$) perturbation is related to DIC changes and air–sea CO_2 flux (F_{CO_2}). The $\mathrm{DIC_{AIR-SEA\ EX}}$ (μmol kg^{-1} d^{-1}) is estimated via the change in the water column DIC inventory as follows:

$$\mathrm{DIC_{AIR-SEA\,EX}} = \frac{k \times s \times (p\mathrm{CO_{2sw}} - p\mathrm{CO_{2air}})}{h \times \rho}, \quad (8)$$

where $pCO_{2sw} - pCO_{2air}$ is the difference in atmospheric and seawater pCO_2 calculated from the buoy measurements, s (mol kg^{-1} atm^{-1}) is the solubility of CO_2 per unit volume of seawater (Weiss, 1974), k (m s^{-1}) is the transfer velocity as a

function of wind speed at 10 m above mean sea level, h is the water column depth (m), and ρ is the seawater density (kg m^{-3}). The transfer velocity–wind speed relationship used was described by Wanninkhof (2014). The net oxygen air–sea flux (F_{O_2}) was calculated similarly to F_{CO_2} (see Supporting Information Text S4 for further details). As a convention in this paper, positive O_2 and CO_2 fluxes represent transfers from the ocean to the atmosphere.

Biology

The biological processes affecting pCO_{2sw} (∂pCO_{2BIO}) were estimated as the residual of the remainder of the other terms in the mass conservation equation (Eq. 3) to close the system. The Revelle factor (β, $\partial \ln pCO_{2sw}/\partial \ln$ DIC) was used to convert changes in ∂pCO_{2BIO} to changes in DIC (∂DIC_{BIO}) using the relation between pCO_{2sw} and DIC as defined by Revelle and Suess (1957). Discrete pH and TA measurements were used to calculate the bottle pCO_{2sw}, DIC, and β values using the CO2SYS program and the same dissociation constants used for the autonomous measurements. The partial change in DIC due to pCO_{2sw} (DIC/$pCO_{2sw} \times \beta$, μmol kg^{-1} μatm^{-1}) was linearly related to temperature (Supporting Information Fig. S3). The ∂pCO_{2BIO} was converted to ∂DIC_{BIO} (μmol kg^{-1}) according to the following relationships for La Parguera and Cheeca Rocks:

$$\frac{\partial DIC_{BIO}}{\partial t} LP\,(\pm 1) = 102 \times SST - 2.1, \quad (9)$$

$$\frac{\partial DIC_{BIO}}{\partial t} CR\,(\pm 4) = 88.7 \times SST - 1.6, \quad (10)$$

where $\pm$ 1 and $\pm$ 4 are the RMSEs of the derived quantity. In this study, the ∂DIC_{BIO} was assumed to come from the combined effects of organic matter formation and remineralization together with calcium carbonate precipitation and dissolution:

$$\frac{\partial DIC_{BIO}}{\partial t} = \frac{\partial DIC_{NEP}}{\partial t} + \frac{\partial DIC_{NEC}}{\partial t}. \quad (11)$$

The changes in oxygen due to biology (O_{2BIO}) were constrained by removing the effects of solubility using oxygen at saturation [O_{2sat}] as a function of temperature and salinity (Weiss, 1970). The change in oxygen due to biological production was then calculated as [O_{2BIO}] = [O_{2obs}] − [O_{2sat}].

NEP and NEC rates

The net daily changes in oxygen due to organic production (∂O_{2NEP}) are defined as follows:

$$\frac{\partial O_{2NEP}}{\partial t} = \frac{\partial O_{2BIO}}{\partial t} - \frac{\partial O_{2GAS}}{\partial t}, \quad (12)$$

where ∂O_{2BIO} is the observed daily change in oxygen concentration (O_{2BIO}, mmol m^{-3}) due to biological production. The ∂O_{2GAS} (mmol m^{-2} d^{-1}) is the oxygen change due to F_{O_2} and corrected for bubble flux (more information in Supporting Information Text S4). The changes in ∂O_{2NEP} were converted to DIC changes (∂DIC_{NEP}) using the stoichiometric metabolic quotient (Q) typically assumed (McGillis et al. 2011; Takeshita et al. 2016) for coral reef ecosystems ($Q = 1$); that is, for each oxygen molecule consumed, a carbon molecule is produced. An internal analysis was performed using different values of Q, ranging from 0.5 to 1.5 (Bolden et al. 2019), to address potential systematic errors introduced in the metabolic calculations (Supporting Information Text S5 and Fig. S3).

NEC is estimated as follows:

$$\frac{\partial DIC_{NEC}}{\partial t} = \frac{\partial DIC_{BIO}}{\partial t} - \frac{\partial DIC_{NEP}}{\partial t}. \quad (13)$$

We subsequently use the terms net autotrophy (net photosynthesis) or net calcification to refer to values of NEP (production − respiration) or NEC (calcification − dissolution) that are greater than zero; similarly, we use the terms net heterotrophy (net respiration) and net dissolution to refer to values of NEP or NEC that are less than zero.

Uncertainty assessment

Model errors for the pCO_{2sw} and DIC mass budget variables, as well as NEP and NEC, were estimated using Monte Carlo simulations (Supporting Information Table S2). Before the Monte Carlo simulations, a Kolmogorov–Smirnov test was performed on each of the model variables to verify that the data were normally distributed. Random normal distributions of each variable were generated using the MATLAB function *randn* (MATLAB 2019a, MathWorks). Sampling was repeated 1000 times to establish the final uncertainty, mean, and standard deviation for each simulation. NEC uncertainties included uncertainties from pCO_{2sw} and NEP. The uncertainty in the gas exchange coefficient was estimated to be 30% (Wanninkhof, 2014).

Results

Seasonal physical and biological drivers of pCO_{2sw}

The results from the 1D mass balance model showed that the seasonal amplitudes in ∂pCO_{2OBS} were less pronounced at La Parguera (25 μatm) than at Cheeca Rocks (100 μatm) because of latitudinal differences in temperature as well as differences in biological composition between the sites (Fig. 3). At Cheeca Rocks, the biological activity was the largest contributor to the observed pCO_{2sw} variability, with counteracting effects of solubility (temperature and salinity) and physical transport (air–sea CO_2 gas exchange and horizontal mixing). ∂pCO_{2BIO} at Cheeca Rocks varied seasonally by 138 μatm, with a maximum of 75 μatm in November and a minimum of −63 μatm in April. The values of ∂pCO_{2SOL} at Cheeca Rocks ranged from −13 μatm in January to +42 μatm in August

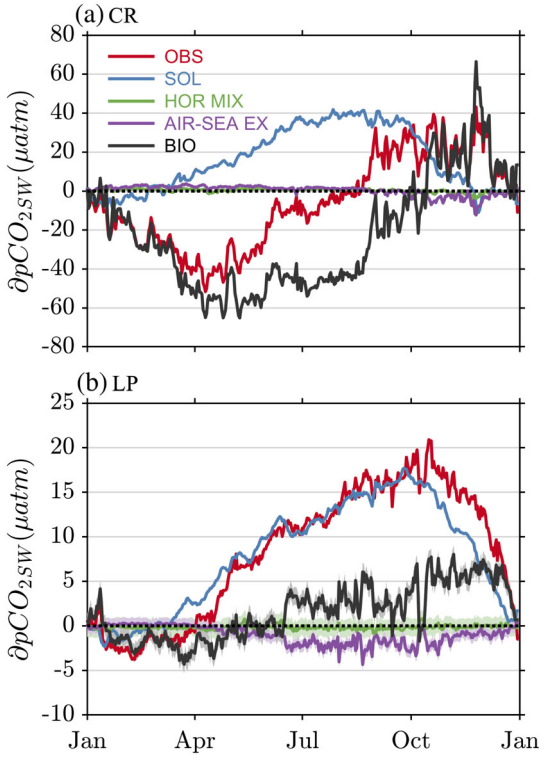

Fig. 3. Cumulative seasonal changes in surface pCO_{2sw} (δpCO_{2sw}; μatm) are based on contributions from solubility, physical transport, and biological processes for Cheeca Rocks (**a**) and La Parguera (**b**). The daily average and model uncertainties (Supporting Information Table S2) in the composite year are represented with solid lines and shaded bounds, respectively. Observations and model results are shown in each panel as observed pCO_2 values (OBS; red), effects of temperature and salinity variability (SOL; blue), effects of horizontal mixing (HOR MIX; green), effects of air–sea exchange (AIR–SEA EX; purple), and effects of biological activity (BIO; black).

(Fig. 3). The annual range of $\partial pCO_{2AIR-SEA\ EX}$ was from -13 μatm in the winter to $+4$ μatm in the fall; this corresponded to a decrease in water column DIC of approximately 10 μmol kg^{-1} during the fall. $\partial pCO_{2HOR\ MIX}$ ranged from -4 to 2 μatm throughout the year, with a small but significant seasonal change ($t = 6.4$, df $= 364$, p-value < 0.05) between winter/spring and summer/fall.

At La Parguera, ∂pCO_{2SOL} ranged from -2 to 18 μatm, similar to the range of ∂pCO_{2OBS} (Fig. 3). The solubility and biological effects on pCO_{2sw} were similar to those typically observed in the open ocean of the Caribbean region (Wanninkhof et al. 2019). However, at La Parguera, the biological counteracting effects were smaller relative to those at Cheeca Rocks (Supporting Information Fig. S5). ∂pCO_{2BIO} varied from -4 μatm in March to 7 μatm in November. ∂pCO_{2BIO} was negative from mid-January to mid-June and positive from July to December. $\partial pCO_{2HOR\ MIX}$ and $\partial pCO_{2AIR-SEA\ EX}$ showed no significant seasonal changes, and we found the contributions of both to be negligible (< 1 μatm) throughout the year.

Annual and seasonal net ecosystem metabolism

On an annual basis, both sites were net heterotrophic and net dissolving (Table 1), with occasional periods of net calcification and net autotrophy (Fig. 4). La Parguera and Cheeca Rocks showed similar ($t = -1.0$, df $= 22$, p-value $= 0.32$) monthly rates of NEP and NEC. The magnitude and direction of the daily NEP and NEC were also similar at both stations (Fig. 4). The net rates of respiration ($-$NEP) and dissolution ($-$NEC) were approximately 1.5 times higher during the summer (July and August) at La Parguera than at Cheeca Rocks. Photosynthesis (+NEP) and calcification (+NEC) were higher and more variable at Cheeca Rocks on an annual basis. The annual cycles of NEP and NEC at both sites indicate that most of the net organic carbon fixation and calcification occurred from December to May, with higher values from January to March. In July and August, NEP and NEC slightly increased at Cheeca Rocks.

The census-based budgets (gross production – bioerosion) were estimated at both locations (Supporting Information Text S6). Even though the census-based NEC was greater at the Cheeca Rocks due to the high coral biomass (Table 1), our chemistry-based NEC over a diurnal cycle likely represented processes from a mix of fine-grained $CaCO_3$ sediments, isolated hard and soft corals, and seagrass (Fig. 1). The census-based NEC at Cheeca Rocks is slightly smaller (2.78 kg $CaCO_3$ m^{-2} yr^{-1}) if we include abiotic dissolution (-0.11 ± 0.12 kg $CaCO_3$ m^{-2} yr^{-1}). The average biologically mediated dissolution of $CaCO_3$ from bioeroding sponges, microbioerosion, parrotfishes, and urchins at Cheeca Rocks was -1.27 kg m^{-2} yr^{-1}, which would enhance chemical dissolution. This was higher than that at La Parguera, where the total bioerosion was estimated at -0.51 kg $CaCO_3$ m^{-2} yr^{-1}. At La Parguera the census (1.0 ± 1.6 kg $CaCO_3$ m^{-2} yr^{-1}) and chemistry (-0.68 ± 0.91 kg $CaCO_3$ m^{-2} yr^{-1}) NEC annual means showed that the forereef is accreting, albeit minimally, and with high variability (Table 1). The census-based abiotic dissolution at La Parguera is estimated as -0.24 ± 0.07 kg $CaCO_3$ m^{-2} yr^{-1}.

The total uncertainties in NEP and NEC calculations were 38% and 46% at La Parguera and 34% and 60% at Cheeca Rocks, respectively (Supporting Information Table S2). These uncertainties are associated with the uncertainties in the gas exchange coefficient and the TA model. The seasonal amplitudes of NEP and NEC were significant ($t = 1.97$, df $= 365$, p-value < 0.05) despite the model uncertainties for both sites. Note that rather than providing values for a certain date, our mass balance approach yielded a climatological assessment of NEP and NEC.

This Modeling caveats and sampling limitations that should be considered include the use of stoichiometric metabolic quotient (Supporting Information Text S7). Even though the magnitude of NEP rate varied based on the stoichiometric metabolic quotient, the seasonal and annual trends did not change (Supporting Information Fig. S4). We assumed the systematic error from the choice of the metabolic quotient to be negligible compared to the large natural variability at these sites. The model was also rerun using oxygen data from an optode

Table 1. NEP and NEC using census- and chemistry-based approaches. The range is shown for the chemistry-based NEC. The annual mean (± uncertainty) is shown for the census-based NEC. Rates are expressed in units of kg $CaCO_3$ m^{-2} yr^{-1} or kg C m^{-2} yr^{-1} using a molecular weight of calcium carbonate (100.09 g mol^{-1}) and carbon (12 g mol^{-1}) for NEC and NEP, respectively.

Study	Location	NEC kg $CaCO_3$ m^{-2} yr^{-1}	NEP kg C m^{-2} yr^{-1}	Coral/calcifier cover (%)	Reef type/method
McGillis et al. (2011)	Puerto Rico		−0.2 to (−0.15)	10	Forereef/enclosure and boundary layer
Bates et al. (2010)	Bermuda	−0.8 to 3.8	−0.5 to 1.0	21	Barrier reef and lagoon
Courtney et al. (2016)	Bermuda	2.2 to 2.3		26	Rim reef, census,* and chemical
Muehllehner et al. (2016)	Florida	−0.3 to 0.6	−0.14 to 0.27	2–7	Patch reefs, Be-7
This study	Florida	−3.7 to 1.9	−0.28 to 0.11	2–7	Patch reefs, chemistry
This study	Florida	2.9 ± 0.9		30	Patch reefs, census†
This study	Puerto Rico	−3.1 to 0.8	−0.38 to 0.10	10–11	Fore-reef/lagoon, chemistry
This study	Puerto Rico	1.0 ± 1.6		11	Fore-reef slope, census†

*Bioerosion is not included.
†Abiotic dissolution is not included.

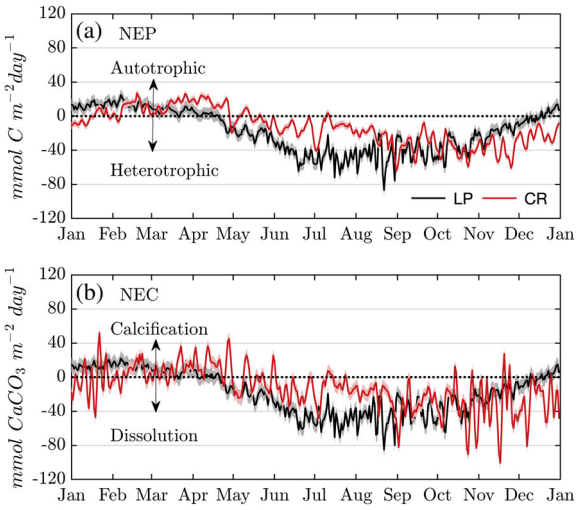

Fig. 4. Annual composites based on daily averages of modeled (**a**) NEP (mmol C m^{-2} d^{-1}) and (**b**) NEC (mmol $CaCO_3$ m^{-2} d^{-1}) for Cheeca Rocks (red) and La Parguera (black). The daily average and model uncertainties in the composite year are represented with solid lines and shaded bounds, respectively. NEP < 0 is representative of net heterotrophy/respiration, and NEP > 0 indicates net autotrophy/photosynthetic. NEC > 0 indicates net calcification, and NEC < 0 indicates net dissolution.

sensor to demonstrate the robust quality of our NEP rates using the post-corrected MAX-250+ oxygen measurements (Supporting Information Fig. S6). The observed NEP differences between the two sensors, and the subsequent effects on NEC, were not statistically different (t_{NEP} = 0.2, df = 361, p-value = 0.84).

Discussion

Validation and comparison with other Atlantic–Caribbean reef areas

There is strong evidence for decreasing carbonate production, coral cover, and biomass of dominant reef-building species throughout the Caribbean and Atlantic regions (Perry et al. 2013). NEC and NEP from this method were validated using census-based budgets and chemistry-based turbulent flux and TA anomaly techniques during short-term surveys at both locations (Supporting Information Figs. S7–S9). Our results agreed with the critical transition zone suggested by Perry et al. (2013), where coral reefs with less than 10% live coral cover typically start to move into a state of net erosion (Supporting Information Fig. S10). The low chemistry-based NEC (Table 1) are not particularly anomalous when compared with the average NEC ranges reported for forereef areas in the Atlantic (0.9–2.7 kg $CaCO_3$ m^{-2} yr^{-1}; Vecsei, 2004) and given the variability (> ±50%) reported for census-based approaches.

We expect that other significant TA and DIC fluxes from organic matter production (Kim and Lee, 2009), anaerobic sediment diagenesis (Yamamoto et al. 2015), $CaCO_3$ sediment calcification/dissolution (Stoltenberg et al. 2021), and nutrient transformation in macroalgae, sediments, and plankton (Wolf-Gladrow et al. 2007) were also integrated into our metabolic measurements. While these assumptions do not affect our calculations, they need to be considered when comparing our results with those of previous studies and for other reef areas. Differences with other studies can be related to several factors, including the method used (e.g., mesocosms, gradient flux, Eulerian, Lagrangian, and census-based), benthic communities, water depth, environmental feedback, hydrodynamics, reef morphology, and spatiotemporal scales. Another possibility is that there is a real decline in NEC in these systems, considering some of these studies are from a decade ago.

Potential drivers related to benthic and water column processes

Our method is a powerful tool for determining seasonal and interannual net ecosystem metabolism changes in the field. NEC results suggest that $CaCO_3$ dissolution can play a large role in reef-scale NEC in areas with low % live coral. Both

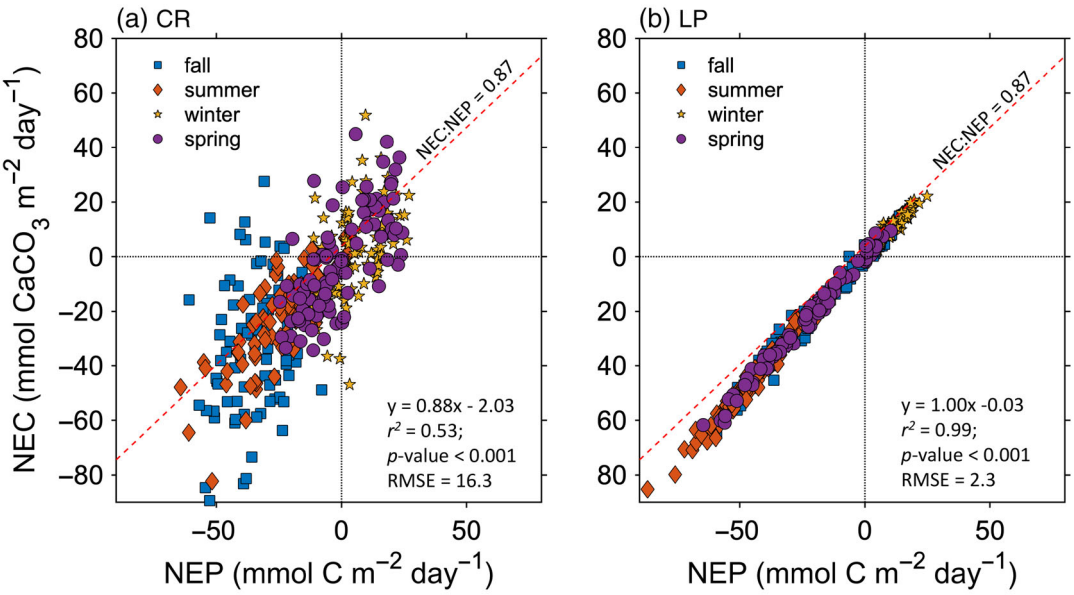

Fig. 5. Seasonal NEC (mmol $CaCO_3$ m^{-2} d^{-1}) vs. NEP (mmol C m^{-2} d^{-1}) for (**a**) Cheeca Rocks and (**b**) La Parguera. The blue square (fall), orange diamond (summer), yellow star (winter), and purple circle (spring) symbols represent the different seasons. The red dashed line represents a theoretical NEC : NEP ratio of approximately 0.87, which maintains an approximately constant Ω_{arag}. Higher slopes (NEC > NEP) decrease Ω_{arag}, and lower slopes (NEC < NEP) increase Ω_{arag}.

sites show net dissolution on an annual basis and a short window (~ 4 months) of net calcification. This window consistently decreased after 2014 at both sites and ranged throughout the time series from 2 to 3.5 (La Parguera) and 2 to 4.5 (Cheeca Rocks) months (Supporting Information Fig. S11). Potential drivers for this decline include the deterioration of coral communities in the Florida Reef Tract (Lirman et al. 2011; Manzello, 2015; Precht et al. 2016) and at La Parguera (Weil et al. 2009) that have caused poor reef health conditions and facilitated shifts to macroalgal dominance reefs.

At Cheeca Rocks, dissolution rates appeared to increase concomitantly with the seagrass biomass and production, which peaked in summer and was at a minimum in winter (Fourqurean et al. 2001; Burdige and Zimmerman, 2002). Microbial decomposition of organic matter can also enhance metabolic dissolution through oxic respiration (Cyronak and Eyre, 2016). Respiration rates at Cheeca Rocks may be fueled by seagrass-derived detritus, seagrass secession, sediment remineralization, and dissolved organic carbon excreted from living leaves, rhizomes, and roots and leached from decomposing tissues (Duarte and Krause-Jensen, 2017). The increases in the biomass and productivity of macroalgae (Collado-Vides et al. 2005) and seagrasses (Lirman and Biber, 2000) from winter to early summer coincide with our highest NEP.

At La Parguera, dissolution is likely generated within the carbonate sediments, coral reef framework, and coral rubble. Shallowness and long residence times at La Parguera site can also increase the accumulation of TA flux from the dissolution of carbonate sediments and coral framework. We hypothesized the mangroves are one of the major organic C sources during the fall in La Parguera. The observed heterotrophic conditions coincided with the wet season, the seasonal decrease in salinity caused by the remote influx of freshwater originating from the Orinoco and Amazon River plumes (Corredor and Morell, 2001), and the frequent occurrence of extensive mats of *Sargassum* washing up in coastal areas (Wang et al. 2019). We hypothesized that the strong mixing and nutrient supply to the surface in the winter could support positive NEP.

The potential effects of temperature driving increased rates of respiration in the summertime were more evident at La Parguera than at Cheeca Rocks (Supporting Information Fig. S12). At La Parguera, NEP and NEC were negatively correlated with temperature ($r^2 = 0.77$), whereas at Cheeca Rocks correlation with temperature was 0.20. The NEP seasonal cycle at both locations may be driven by either a recent decrease in new nutrients leading to overall lower annual NEP or an increase in organic matter delivery driving overall higher levels of respiration that decrease NEP. Additional work should be focused on understanding other environmental drivers and regional sources of nutrients and organic matter in both locations.

Relationship between NEC and NEP

Significant correlations between NEC and NEP have been observed in previous studies in the field on hourly (McMahon

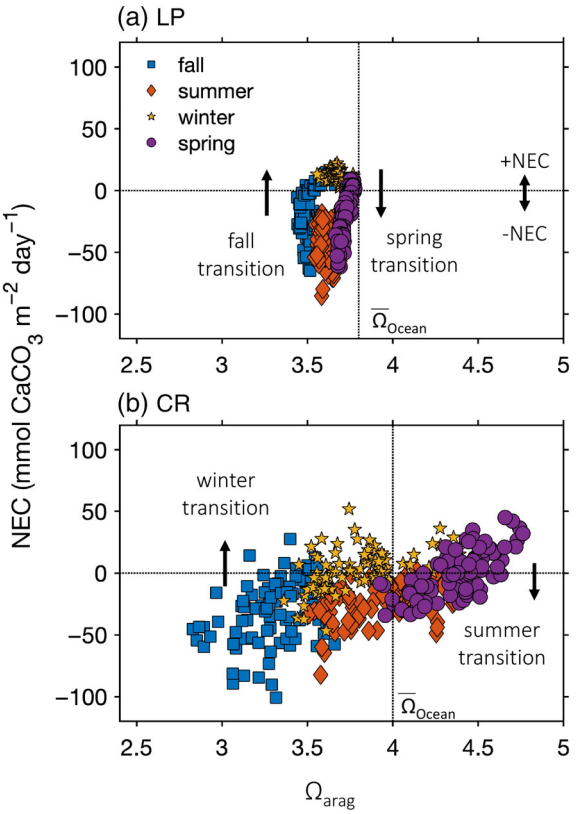

Fig. 6. Seasonal NEC (mmol $CaCO_3$ m^{-2} d^{-1}) for La Parguera (**a**) and Cheeca Rocks (**b**) relative to Ω_{arag}. The gray horizontal dashed line indicates zero NEP/NEC and the vertical line the mean oceanic Ω_{arag} ($\overline{\Omega}_{ocean}$). The black arrows represent the approximate area and direction at which NEC becomes negative or positive (i.e., the seasonal transition zone between trophic status). In situ bottle TA and DIC samples from seasonal cruises in the Caribbean Sea and Florida Straits were used to calculate $\overline{\Omega}_{ocean}$.

et al. 2013; Albright et al. 2015; DeCarlo et al. 2017) and daily integrated metabolic rates (Muehllehner et al. 2016; Takeshita et al. 2016). To our knowledge, this is the first analysis of both, NEP and NEC, using continuous long-term pCO_2 and oxygen measurements. The linear relationships between NEC and NEP (Fig. 5) showed a significant slope (± standard error) of 1.00 ± 0.005 (t = 205.2, df = 364, p-value < 0.05) for La Parguera and 0.88 ± 0.04 (t = 16.5, df = 364, p-value < 0.05) for Cheeca Rocks. Our seasonal net ecosystem metabolic rates suggest that NEP is the primary driver of NEC at La Parguera (r^2_{LP} = 0.99), and partially explain some of the variations at Cheeca Rocks (r^2_{CR} = 0.53, p-value < 0.01). This linear correlation is consistent with previous studies and with the hypothesis that organic carbon dynamics play an important role in the modulation of the carbonate chemistry in reef waters (Gattuso et al. 1998). Because of the correlation between NEC and NEP, the effects of ocean acidification on NEC could be masked by other processes that influence net primary production on longer timescales (e.g., nutrients, carbon, and temperature). The strong coupling between NEP and NEC can also cause hysteresis (Meléndez et al. 2020) between NEC and seawater surface saturation states that complicates the use of first-order derivations of NEC-Ω_{arag} (Silverman et al. 2007). Note that a high correlation coefficient was likely because NEC was partially dependent on NEP in our model (Eq. 13), although pCO_{2sw} and oxygen measurements were independent. To better de-convolve the influence of NEP on NEC, it may be necessary to independently calculate more accurate high-frequency fluxes of TA, which was not possible using our data set.

The threshold NEP rate corresponding to the annual zero NEC (NEC = 0) was estimated from the intercept between NEP and NEC. The intercept at Cheeca Rocks was significantly (p-value < 0.05) different than zero at −2.03 ± 0.99 mmol m^{-2} d^{-1}. Above this value of annual NEP, we would expect a positive annual NEC at Cheeca Rocks. While at La Parguera the intercept (−0.03 ± 0.15 mmol m^{-2} d^{-1}) was not significantly different from zero (p-value = 0.86).

Ecosystem metabolism and Ω_{arag}

The relationships of NEC with Ω_{arag} provide a better understanding of the changes in Ω_{arag} due to the combined effects of the rates of change in NEC and NEP on seasonal timescales (Andersson and Gledhill, 2013). We defined the x-intercept (Fig. 5) as the seasonal shifts or threshold points at which NEC was zero. This represents the point at which dissolution exceeded calcification. Figure 6 shows that at Cheeca Rocks the Ω_{arag} where NEC is zero was 4.00 ± 0.02, which agreed with the results of Muehllehner et al. (2016). Results suggested that Ω_{arag} was not the primary driver of NEC at La Parguera, while at Cheeca Rocks, the linear correlation between NEC and Ω_{arag} showed that 30% of the variance can be explained by Ω_{arag}. At La Parguera, the two transitions where NEC was zero occurred at 3.75 in April (spring) and 3.50 in December (fall).

Results suggest that systems such as Cheeca Rocks with a low correlation between NEC and NEP (Fig. 5) and where the organic carbon cycle is relatively balanced (i.e., NEP = 0) could have weaker hysteresis and therefore a significant correlation between NEC and Ω_{arag}. The seasonal hysteresis suggests that long-term observations of nearshore seawater Ω_{arag} may not be a good predictor of long-term changes in NEC, which has also been suggested by recent diurnal studies (Cyronak et al. 2013; McMahon et al. 2013; Shaw et al. 2015).

Conclusions

This study derived seasonal changes in NEC and NEP under naturally variable in situ conditions using a mass balance approach at La Parguera and Cheeca Rocks. The 1D mass balance approach used nearly a decade of long-term and high-frequency pCO_{2sw} and oxygen observations as proxies to decouple NEP and NEC of communities close (< 5 km) to the buoys. Both sites were net heterotrophic and showed net dissolution on an annual scale. The average (± standard deviation)

NEC ranged from 11 ± 5 and 13 ± 10 mmol $CaCO_3$ m^{-2} d^{-1} in winter to −45 ± 14 and −18 ± 11 mmol $CaCO_3$ m^{-2} d^{-1} in summer at La Parguera and Cheeca Rocks, respectively. The average NEP ranged from 11 ± 5 and 8 ± 6 mmol C m^{-2} d^{-1} in winter to −45 ± 13 and −20 ± 10 mmol C m^{-2} d^{-1} in summer at La Parguera and Cheeca Rocks, respectively. Results suggest that tropical Caribbean reef ecosystems likely exhibit extended periods of net dissolution of highly soluble carbonate minerals based on the similarities in their environmental characteristics.

Our observations showed that NEP, as diagnosed by dissolved oxygen, is a good predictor of NEC in these systems. As such, it is of the utmost importance for monitoring programs to integrate oxygen sensors, as well as changes in the net ecosystem processes, which often regulate local chemistry conditions. Observations support recent studies that show that Ω_{arag} probably is not the most informative predictor of long-term NEC outside of a controlled experiment. The 1D model can be tested and applied in other reef regions with similar buoys and auxiliary carbonate data to better understand the ocean acidification conditions over different oceanic settings.

References

Albright, R., J. Benthuysen, N. Cantin, K. Caldeira, and K. Anthony. 2015. Coral reef metabolism and carbon chemistry dynamics of a coral reef flat. Geophys. Res. Lett. **42**: 3980–3988. doi:10.1002/2015GL063488

Andersson, A. J., and D. Gledhill. 2013. Ocean acidification and coral reefs: Effects on breakdown, dissolution, and net ecosystem calcification. Ann. Rev. Mar. Sci. **5**: 321–348. doi:10.1146/annurev-marine-121211-172241

Andersson, A. J., and others. 2019. Ecological and socioeconomic strategies to sustain Caribbean coral reefs in a high-CO_2 world. Reg. Stud. Mar. Sci. **29**: 100677. doi:10.1016/j.rsma.2019.100677

Barbero, L. & others 2019. Third Gulf of Mexico ecosystems and carbon cycle (GOMECC-3) cruise technical report. Atlantic Oceanographic and Meteorological Laboratory. https://doi.org/10.25923/y6m9-fy08

Bates, N. R., A. Amat, and A. J. Andersson. 2010. Feedbacks and responses of coral calcification on the Bermuda reef system to seasonal changes in biological processes and ocean acidification. Biogeosciences **7**: 2509–2530. doi:10.5194/bg-7-2509-2010

Bates, N. R., M. H. P. Best, K. Neely, R. Garley, A. G. Dickson, and R. J. Johnson. 2012. Detecting anthropogenic carbon dioxide uptake and ocean acidification in the North Atlantic Ocean. Biogeosciences **9**: 2509–2522. doi:10.5194/bg-9-2509-2012

Bolden, I. W., J. P. Sachs, and A. C. Gagnon. 2019. Temporally-variable productivity quotients on a coral atoll: Implications for estimates of reef metabolism. Mar. Chem. **217**: 103707. doi:10.1016/j.marchem.2019.103707

Burdige, D. J., and R. C. Zimmerman. 2002. Impact of sea grass density on carbonate dissolution in Bahamian sediments. Limnol. Oceanogr. **47**: 1751–1763.

Cai, W.-J., X. Hu, W.-J. Huang, L.-Q. Jiang, Y. Wang, T.-H. Peng, and X. Zhang. 2010. Alkalinity distribution in the western North Atlantic Ocean margins. J. Geophys. Res. **115**: C08014. doi:10.1029/2009JC005482

Collado-Vides, L., L. M. Rutten, and J. W. Fourqurean. 2005. Spatiotemporal variation of the abundance of calcareous green macroalgae in the Florida keys: A study of synchrony within a macroalgal functional-form group. J. Phycol. **41**: 742–752.

Corredor, J. E., and J. M. Morell. 2001. Seasonal variation of physical and biogeochemical features in eastern Caribbean Surface Water. J. Geophys. Res. **106**: 4517–4525. doi:10.1029/2000JC000291

Courtney, T. A., and others. 2016. Comparing chemistry and census-based estimates of net ecosystem calcification on a rim reef in Bermuda. Front. Mar. Sci. **3**: 181. doi:10.3389/fmars.2016.00181

Cyronak, T., I. R. Santos, A. McMahon, and B. D. Eyre. 2013. Carbon cycling hysteresis in permeable carbonate sands over a diel cycle: Implications for ocean acidification. Limnol. Oceanogr. **58**: 131–143.

Cyronak, T., K. G. Schulz, I. R. Santos, and B. D. Eyre. 2014. Enhanced acidification of global coral reefs driven by regional biogeochemical feedbacks. Geophys. Res. Lett. doi: **41**: 5538–5546. 10.1002/2014GL060849

Cyronak, T., and B. D. Eyre. 2016. The synergistic effects of ocean acidification and organic metabolism on calcium carbonate ($CaCO_3$) dissolution in coral reef sediments. Mar. Chem. **183**: 1–12. doi:10.1016/j.marchem.2016.05.001

DeCarlo, T. M., A. L. Cohen, G. T. F. Wong, F. Shiah, S. J. Lentz, K. A. Davis, K. E. F. Shamberger, and P. Lohmann. 2017. Community production modulates coral reef pH and the sensitivity of ecosystem calcification to ocean acidification. J. Geophys. Res. Ocean. **122**: 745–761. doi:10.1002/2016JC012326

Dickson, A. G. 1990. Thermodynamics of the dissociation of boric acid in potassium chloride solutions from 273.15 to 318.15 K. J. Chem. Eng. Data **35**: 253–257.

Duarte, C. M., and others. 2013. Is ocean acidification an open-ocean syndrome? Understanding anthropogenic impacts on seawater pH. Estuar. Coasts: **36**: 221–236. doi:10.1007/s12237-013-9594-3

Duarte, C. M., and D. Krause-Jensen. 2017. Export from seagrass meadows contributes to marine carbon sequestration. Front. Mar. Sci. **4**: 13.

Fassbender, A. J., C. L. Sabine, and K. M. Feifel. 2016. Consideration of coastal carbonate chemistry in understanding biological calcification. Geophys. Res. Lett. **43**: 4467–4476. doi:10.1002/2016GL068860

Flagg, C. N., J. A. Vermersch, and R. C. Beardsley. 1976. 1974 MIT New England shelf dynamics experiment (March, 1974). Data report, Part II: Moored array, MIT Rep. 76-1.

Fourqurean, J. W., A. Willsie, C. D. Rose, and L. M. Rutten. 2001. Spatial and temporal pattern in seagrass community composition and productivity in south Florida. Mar. Biol. **138**: 341–354. doi:10.1007/s002270000448

Friedlingstein, P., and others. 2019. Global carbon budget 2019. Earth Syst. Sci. Data **11**: 1783–1838. doi:10.5194/essd-11-1783-2019

Gardner, T. A., I. M. Côté, J. A. Gill, A. Grant, and A. R. Watkinson. 2003. Long-term region-wide declines in Caribbean corals. Science **301**: 958–960. doi:10.1126/science.1086050

Gattuso, J.-P., M. Frankignoulle, and R. Wollast. 1998. Carbon and carbonate metabolism in coastal aquatic ecosystems. Annu. Rev. Ecol. Syst. **29**: 405–434. doi:10.1146/annurev.ecolsys.29.1.405

Gledhill, D. K., R. Wanninkhof, F. J. Millero, and M. Eakin. 2008. Ocean acidification of the Greater Caribbean Region 1996–2006. J. Geophys. Res. **113**: 1–11. doi:10.1029/2007JC004629

Gruber, N., C. D. Keeling, and T. F. Stocker. 1998. Carbon-13 constraints on the seasonal inorganic carbon budget at the BATS site in the northwestern Sargasso Sea. Deep Sea Res. Part I Oceanogr. Res. Pap. **45**: 673–717. doi:10.1016/S0967-0637(97)00098-8

Jones, J. A. 1977. Morphology and development of southeastern Florida patch reefs, p. 231–235. *In* Proceedings Third International Coral Reef Symposium. **2**: Proc 3rd Int Coral Reef Symp.

Kendall, M.S, M.E. Monaco, K.R. Buja, J.D. Christensen, C.R. Kruer, M. Finkbeiner & R.A. Warner1 2001. Methods used to map the benthic habitats of Puerto Rico and the U.S. Virgin Islands. NOAA Technical Memorandum NOS NCCOS CCMA 152 (On-line). Available from http://biogeo.nos.noaa.gov/projects/mapping/caribbean/startup.htm.

Kim, H., and K. Lee. 2009. Significant contribution of dissolved organic matter to seawater alkalinity. Geophys. Res. Lett. **36**: L20603. doi:10.1029/2009GL04027

Lee, K., and others. 2006. Global relationships of total alkalinity with salinity and temperature in surface waters of the world's oceans. Geophys. Res. Lett. **33**: L19605. doi:10.1029/2006GL027207

Lirman, D., and P. Biber. 2000. Seasonal dynamics of macroalgal communities of the northern Florida reef tract. Bot. Mar. **43**: 305–314. doi:10.1515/BOT.2000.033

Lirman, D., and others. 2011. Severe 2010 cold-water event caused unprecedented mortality to corals of the Florida reef tract and reversed previous survivorship patterns. PLoS One **6**: e23047. doi:10.1371/journal.pone.0023047

Lueker, T. J., A. G. Dickson, and C. D. Keeling. 2000. Ocean pCO_2 calculated from dissolved inorganic carbon, alkalinity, and equations for K_1 and K_2: Validation based on laboratory measurements of CO_2 in gas and seawater at equilibrium. Mar. Chem. **70**: 105–119. doi:10.1016/S0304-4203(00)00022-0

Manzello, D. P. 2015. Rapid recent warming of coral reefs in the Florida keys. Sci. Rep. **5**: 16762. doi:10.1038/srep16762

Massaro, R. F. S., E. H. De Carlo, P. S. Drupp, F. T. Mackenzie, S. M. Jones, K. E. Shamberger, C. L. Sabine, and R. A. Feely. 2012. Multiple factors driving variability of CO_2 exchange between the ocean and atmosphere in a tropical coral reef environment. Aquat. Geochem. **18**: 357–386. doi:10.1007/s10498-012-9170-7

McGillis, W. R., C. Langdon, B. Loose, K. K. Yates, and J. Corredor. 2011. Productivity of a coral reef using boundary layer and enclosure methods. Geophys. Res. Lett. **38**: 1–5. doi:10.1029/2010GL046179

McMahon, A., I. R. Santos, T. Cyronak, and B. D. Eyre. 2013. Hysteresis between coral reef calcification and the seawater aragonite saturation state. Geophys. Res. Lett. **40**: 4675–4679. doi:10.1002/grl.50802

Meléndez, M., and others. 2020. Seasonal variations of carbonate chemistry at two Western Atlantic coral reefs. J. Geophys. Res. Ocean **125**: e2020JC016108. doi:10.1029/2020JC016108

Moyer, R. P., T. S. Viehman, G. A. Piniak, and D. K. Gledhill. 2012. Linking seasonal changes in benthic community structure to seawater chemistry, p. 9–13. *In* Proceedings of the 12th International Coral Reef Symposium, Cairns, Australia.

Mucci, A. 1983. The solubility of calcite and aragonite in seawater at various salinities, temperatures, and one atmosphere total pressure. Am. J. Sci. **283**: 780–799. doi:10.2475/ajs.283.7.780

Muehllehner, N., C. Langdon, A. Venti, and D. Kadko. 2016. Dynamics of carbonate chemistry, production, and calcification of the Florida Reef Tract (2009–2010): Evidence for seasonal dissolution. Global Biogeochem. Cycles **30**: 661–688. doi:10.1002/2015GB005327

Newton, J. A., R. A. Feely, E. B. Jewett, P. Williamson, and J. Mathis. 2015. Global ocean acidification observing network: Requirements and governance plan. Second Edition, https://archimer.ifremer.fr/doc/00651/76343/GOA-ON

Orr, J. C., J.-M. Epitalon, A. G. Dickson, and J.-P. Gattuso. 2018. Routine uncertainty propagation for the marine carbon dioxide system. Mar. Chem. **207**: 84–107. doi:10.1016/j.marchem.2018.10.006

Perry, C. T., G. N. Murphy, P. S. Kench, S. G. Smithers, E. N. Edinger, R. S. Steneck, and P. J. Mumby. 2013. Caribbean-wide decline in carbonate production threatens coral reef growth. Nat. Commun. **4**: 1402. doi:10.1038/ncomms2409

Precht, W. F., B. E. Gintert, M. L. Robbart, R. Fura, and R. van Woesik. 2016. Unprecedented disease-related coral mortality in Southeastern Florida. Sci. Rep. **6**: 31374. doi:10.1038/srep31374

Revelle, R., and H. E. Suess. 1957. Carbon dioxide exchange between atmosphere and ocean and the question of an increase of atmospheric CO_2 during the past decades. Tellus **9**: 18–27. doi:10.3402/tellusa.v9i1.9075

Shadwick, E. H., H. Thomas, K. Azetsu-Scott, B. J. W. Greenan, E. Head, and E. Horne. 2011. Seasonal variability of

dissolved inorganic carbon and surface water pCO_2 in the Scotian shelf region of the Northwestern Atlantic. Mar. Chem. **124**: 23–37. doi:10.1016/j.marchem.2010.11.004

Shaw, E. C., S. R. Phinn, B. Tilbrook, and A. Steven. 2015. Natural in situ relationships suggest coral reef calcium carbonate production will decline with ocean acidification. Limnol. Oceanogr. **60**: 777–788. doi:10.1002/lno.10048

Silverman, J., B. Lazar, and J. Erez. 2007. Effect of aragonite saturation, temperature, and nutrients on the community calcification rate of a coral reef. J. Geophys. Res. Ocean **112**: 1–14. doi:10.1029/2006JC003770

Smith, N. P., and T. N. Lee. 2003. Volume transport through tidal channels in the middle Florida keys. J. Coast. Res. **19**: 254–260.

Stoltenberg, L., K. G. Schulz, C. A. Lantz, T. Cyronak, and B. D. Eyre. 2021. Late afternoon seasonal transition to dissolution in a coral reef: An early warning of a net dissolving ecosystem? Geophys. Res. Lett. **48**: e2020GL090811. doi:10.1029/2020GL090811

Sutton, A. J., and others. 2014. A high-frequency atmospheric and seawater pCO_2 data set from 14 open-ocean sites using a moored autonomous system. Earth Syst. Sci. Data **6**: 353–366. doi:10.5194/essd-6-353-2014

Sutton, A. J., and others. 2019. Autonomous seawater pCO_2 and pH time series from 40 surface buoys and the emergence of anthropogenic trends. Earth Syst. Sci. Data **11**: 421–439. doi:10.5194/essd-11-421-2019

Takahashi, T., J. Olafsson, J. G. Goddard, D. W. Chipman, and S. C. Sutherland. 1993. Seasonal variation of CO_2 and nutrients in the high-latitude surface oceans: A comparative study. Global Biogeochem. Cycl. **7**: 843–878. doi:10.1029/93GB02263

Takeshita, Y., W. McGillis, E. M. Briggs, A. L. Carter, E. M. Donham, T. R. Martz, N. N. Price, and J. E. Smith. 2016. Assessment of net community production and calcification of a coral reef using a boundary layer approach. J. Geophys. Res. Ocean **121**: 5655–5671. doi:10.1002/2016JC011886

Taylor, C., D. Field, J. Vander Pluym, S. Viehman, and E. Ebert. 2018. NCCOS mapping: Seafloor mapping products for the Florida Keys National Marine Sanctuary from 2004-01-01 to 2016-12-31 (NCEI accession 0170215). NOAA National Centers for Environmental Information. Dataset. doi:10.7289/V55B00RZ

van Heuven, S. M. A. C., D. Pierrot, J. W. B. Rae, E. Lewis, and D. W. R. Wallace. 2011. MATLAB program developed for CO_2 system calculations. ORNL/CDIAC-105b. Carbon Dioxide Information Analysis Center, Oak Ridge National Laboratory, US Department of Energy.

Vecsei, A. 2004. A new estimate of global reefal carbonate production including the fore-reefs. Glob. Planet. Change **43**: 1–18. doi:10.1016/j.gloplacha.2003.12.002

Wang, M., C. Hu, B. B. Barnes, G. Mitchum, B. Lapointe, and J. P. Montoya. 2019. The great Atlantic Sargassum belt. Science **365**: 83–87. doi:10.1126/science.aaw7912

Wanninkhof, R. 2014. Relationship between wind speed and gas exchange over the ocean revisited. Limnol. Oceanogr. Methods **12**: 351–362. doi:10.4319/lom.2014.12.351

Wanninkhof, R., J. Triñanes, G. H. Park, D. Gledhill, and A. Olsen. 2019. Large decadal changes in air–sea CO_2 fluxes in the Caribbean Sea. J. Geophys. Res. Ocean **124**: 6960–6982. doi:10.1029/2019JC015366

Weil, E., A. Croquer, and I. Urreiztieta. 2009. Temporal variability and impact of coral diseases and bleaching in La Parguera, Puerto Rico from 2003–2007. Caribb. J. Sci. **45**: 221–246. doi:10.18475/cjos.v45i2.a10

Weiss, R. F. 1970. The solubility of nitrogen, oxygen and argon in water and seawater. Deep Sea Res. Oceanogr. Abstr. **17**: 721–735. doi:10.1016/0011-7471(70)90037-9

Weiss, R. F. 1974. Carbon dioxide in water and seawater: The solubility of a non-ideal gas. Mar. Chem. **2**: 203–215. doi:10.1016/0304-4203(74)90015-2

Wolf-Gladrow, D. A., R. E. Zeebe, C. Klaas, A. Körtzinger, and A. G. Dickson. 2007. Total alkalinity: The explicit conservative expression and its application to biogeochemical processes. Mar. Chem. **106**: 287–300. doi:10.1016/j.marchem.2007.01.006

Xue, L., W.-J. Cai, X. Hu, C. Sabine, S. Jones, A. J. Sutton, L.-Q. Jiang, and J. J. Reimer. 2016. Sea surface carbon dioxide at the Georgia time series site (2006–2007): Air–sea flux and controlling processes. Prog. Oceanogr. **140**: 14–26. doi:10.1016/j.pocean.2015.09.008

Yamamoto, S., H. Kayanne, T. Tokoro, T. Kuwae, and A. Watanabe. 2015. Total alkalinity flux in coral reefs estimated from eddy covariance and sediment pore-water profiles. Limnol. Oceanogr. **60**: 229–241. doi:10.1002/lno.10018

Yates, K. K., and R. B. Halley. 2003. Measuring coral reef community metabolism using new benthic chamber technology. Coral Reefs **22**: 247–255. doi:10.1007/s00338-003-0314-5

Acknowledgments

We acknowledge NOAA's Ocean Acidification Program (OAP), the National Coral Reef Monitoring Program (NCRMP) and the Caribbean Coastal Ocean Observing System (CARICOOS) for the efforts of these sustained time series. We thank anonymous reviewers, Chris Hunt and Christopher Sabine for improving this manuscript with their constructive comments and feedback. This is PMEL contribution 5132.

Conflict of Interest

None declared.

Submitted 08 December 2020
Revised 30 August 2021
Accepted 12 December 2021

Deputy editor: Steeve Comeau